Open Access Library Journal

Application of Discrimination Filter Based on the Polarization to the Surface Wave Records

Nilgun Sayil

Department of Geophysics, Engineering Faculty, Karadeniz Technical University, Trabzon, Turkey
Email: sayil@ktu.edu.tr

Received 2 May 2014; revised 12 June 2014; accepted 24 July 2014

Abstract

As well known, each type of seismic waves has a specific particle motion. The basic surface waves Love and Rayleigh show the particle motions polarized linearly in the transversal-horizontal plane and elliptically in the vertical-radial plane, respectively. Like in the body waves, polarization properties can be used to design the surface wave discrimination filter. The process consists of weighting the amplitudes of vertical (*Z*), radial (*R*) and tangential (*T*) components of the ground motion at each frequency according to the particle motion. The weighting process is applied to entire length of each component for selected window length and moving interval, but weights are not applied to the original phase values. The weighted parts for each window are transformed to the time domain and filtered signals are obtained as the arithmetic average of values of the overlapping points. The method has been applied to the broad-band digital three-component records at stations having about 10° epicenter distances of Bogazici University Kandilli Observatory and Earthquake Research Institute (KOERI) of Erzurum earthquakes and noticed that the window length and moving interval in proportion to epicenter distance affect the results on a large scale. For the cases in which the best results are obtained, it has been determined that the ratio between the window length and moving interval for increased epicenter distances are 3.95, 4.5 and 4.8, respectively.

Keywords

Discrimination Filter, Polarization Properties, Surface Wave

Subject Areas: **Applied Physics, Geophysics, Particle Physics**

1. Introduction

The parameters such as group arrival times, phase angles and amplitude values of surface waves are used to re-

How to cite this paper: Sayil, N. (2014) Application of Discrimination Filter Based on the Polarization to the Surface Wave Records. *Open Access Library Journal*, **1**: e724. http://dx.doi.org/10.4236/oalib.1100724

searching elastic properties of the Earth. The environmental noise, the noise related to signal, the equal sharing of seismic energy between components and the other factors influence discrimination of surface waves forms on seismograms. The differences between polarization properties of surface waves and microseismic noises enable to filter a desired type of surface waves on three components records. Discrimination filter based on the polarization properties can be used to substantially improve the discrimination of surface waves on three components records. The analysis of polarization depended on rectilinearity and directionality properties. These properties provide to design weighting functions for seismic wave discrimination. If the signals of the different components have same phases, they are called as P- or S-waves and have linear movement. If the signals have different phases, they are called as Rayleigh waves and have elliptical movement. Therefore, Rayleigh wave with elliptical particle motion in the vertical-radial plane and Love wave with linear particle motion in the tangential-horizontal plane can be discriminated on seismograms by weighting functions.

The basis of the surface wave discrimination filter depended on polarization properties was explicitly given by [1]. Preliminary research about this subject has been applied by [2]. Later, [3]-[5] have been developed different algorithms related to the polarization analysis. Reference [6] noted that rectilinearity and directionality properties are simply obtained by data covariance matrix. Reference [7] has determined the weighting functions as depend on frequency. References [8] [9] have investigated the data belonging to three component stations network. Reference [10] has applied polarization analysis to multichannel seismic data. Reference [11] applied to surface wave discrimination filter based on polarization properties on long-period three components records of the three major earthquakes with different epicenter distances larger than 40˚. They found that in case of existence of the surface waves having substantially great amplitudes recorded on seismograms, it can be filtered perfectly. Body wave polarization was investigated by [12]-[15]. References [16] [17] have designed to modified weighting functions for epicenter distances smaller than about 20˚ to corresponding with angular distribution of polarization parameters obtained from computed synthetic seismograms and applied to three component earthquake records for discrimination of surface waves. In this study, it has been investigated applicability of the surface wave discrimination filter to the earthquake records having about 10˚ epicenter distances.

2. Surface Wave Discrimination Filter Based on Polarization Properties

This process is a digital procedure for extracting long-period surface wave signals from microseismic noise. The technique is deterministic and means basically to frequency filtering using measurements on particle motion to shape the filter response. Filtering process is performed in the frequency domain-because of dispersive characters of surface waves. The discrete Fourier transforms of vertical, radial and tangential components of the ground motion are computed for a selected window length and moving interval. The amplitude coefficients at each frequency are weighted according to how closely the three-dimensional particle motion pattern at that frequency corresponds to theoretical patterns for Love and Rayleigh waves, arriving from some pre-assigned direction. The weights or adjustments are not applied to the original phase values. Weighted segments for each window are transformed to the time domain, and filtered signal is obtained as the arithmetic average of the overlapping amplitudes.

In application of this process, a long-period greater than 2.0 sec is considered since it has substantially high the signal-to-noise ratios of surface waves which were barely discernible on the unprocessed seismograms. The physical reason for to achieve this filtering lies the inherent spectral difference between the sought-for signals and the background noise. Thus, it is possible to obtain favorable signal-to-noise ratios in the frequency domain from data which appears highly contaminated in the time domain. This spectral difference is generally realizable in the long-period band because of the characteristics of the noise field.

Whereas surface waves from both earthquakes and detonations usually have energy distributed over a broad frequency range, microseismic noise energy tends to be concentrated in two fairly restricted spectral peaks, around periods of 6 sec and 15 sec [18]. In the frequency bands around the microseismic peaks, the particle motion pattern of a low-level signal is confused by the noise (interfering multidirectional Rayleigh, presumably), and the resultant error causes to attenuate those frequencies. However, the rest of the signal spectrum remains relatively uncovered and the reconstructed time traces preserve the basic character and envelope of the whole surface wave train. The spectral concentration of microseismic noise can further be exploited by straightforward elimination of the certain frequencies. The following basic functions are performed:

1) The magnifications of the three digitized seismograph traces (a vertical and two horizontal components) are equalized, then the horizontal axes are rotated so that one component (the “radial”) is in line with the azimuth at which the desired signal is expected to arrive (not necessarily the great circle path). Theoretically, then, one can

expect to seek Rayleigh motion appearing only on the vertical and radial trace $Z(\tau)$ and $R(\tau)$; Love motion should appear only on the transverse trace $T(\tau)$. No correction is done for the seismographs' frequency response; both input and output traces are analogous to the seismogram that would be normally recorded.

2) The rotated traces are divided into simultaneous time segments with length T, then for each three directional components the amplitude, $A_i(\eta f)$ and phase, $\Phi_i(\eta f)$ information are computed by discrete Fourier series as in Equations (1) and (2).

$$A_i(\eta f) = \left[a_i^2(\eta f) + b_i^2(\eta f)\right]^{1/2} \tag{1}$$

$$\Phi_i(\eta f) = \arctan\left[\frac{b_i(\eta f)}{a_i(\eta f)}\right], \qquad \eta = 0,1,2,\cdots,N-1 \tag{2}$$

where $i = Z, R, T$ which represents the vertical, radial and tangential components of the ground motion, respectively. NF, Nyquist Frequency, $f = 1/T$. $a_i(\eta f)$ and $b_i(\eta f)$ are discrete Fourier series coefficients.

3) The apparent horizontal azimuth, $\beta(\eta f)$ of each harmonic is determined by Equation (3), as if both the horizontal components were in phase, in terms of the angle from the radial direction (**Figure 1**). A measure of the eccentricity of the particle motion ellipse, $\psi(\eta f)$ is also calculated by Equation (4), and the phase difference, $\alpha(\eta f)$ between the vertical and radial components is determined by Equation (5).

$$\beta(\eta f) = \arctan\left[\frac{A_T(\eta f)}{A_R(\eta f)}\right] \tag{3}$$

$$\psi(\eta f) = \arctan\left[\frac{A(\eta f)}{A_Z(\eta f)}\right], \quad \left(A(\eta f) = \left[A_R^2(\eta f) + A_T^2(\eta f)\right]^{1/2}\right) \tag{4}$$

$$\alpha(\eta f) = \phi_R(\eta f) - \phi_Z(\eta f) \tag{5}$$

4) The Fourier amplitude coefficients of each direction component, $A_R(\eta f)$, $A_T(\eta f)$ and $A_Z(\eta f)$ are then weighted according to the formulas in Equation (6).

$$\begin{aligned} A'_Z(\eta f) &= A_Z(\eta f)\cdot\cos^M\left[\beta(\eta f)\right]\cdot\cos^K\left[\psi(\eta f)-\theta\right]\cdot\sin^N\left[\alpha(\eta f)\right] \\ A'_R(\eta f) &= A_R(\eta f)\cdot\cos^M\left[\beta(\eta f)\right]\cdot\cos^K\left[\psi(\eta f)-\theta\right]\cdot\sin^N\left[\alpha(\eta f)\right] \\ A'_T(\eta f) &= A_T(\eta f)\cdot\sin^M\left[\beta(\eta f)\right]\cdot\sin^K\left[\psi(\eta f)\right] \end{aligned} \tag{6}$$

where $\sin^N\left[\alpha(nf)\right], \pi \le \alpha(\eta f) \le 2\pi$. $A'_T(\eta f)$, $A'_R(\eta f)$ and $A'_Z(\eta f)$ are the weighted vertical, radial and tangential components of the ground motion. No weights or adjustments are applied to the phase angles. Note that the Z and R components have identical treatment, and that all weighting factors vary from 0 to 1 as powers of sinus or cosinus depending upon the degree to which the particle motion corresponds to pure Love or Rayleigh wave behavior. To date, the most satisfactory results generally have been obtained with the weighting exponents M, K, and N set to are empirically determined as 8, 8 and 4, respectively, operating on segments 128 sec long with a 1/16 (8 sec) time increment [1].

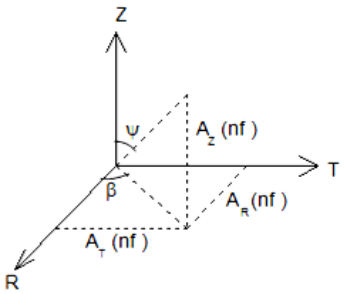

Figure 1. The relation between the apparent horizontal azimuth β, the eccentricity ψ and three orthogonal components of ground motion $A_R(\eta f)$, $A_T(\eta f)$ and $A_Z(\eta f)$.

The effects of the first weighting factors (functions of β) are to attenuate transverse-tending energy on the *Z* and *R* components and radial-tending energy on the *T* component. In other words, in case the motion in the horizontal plane is radial perfectly ($\beta(\eta f) = 0$), it is seen that the amplitude coefficients of the *Z* and *R* components are stable and that of the *T* component are decreased. This situation is also derived from the Rayleigh wave particle motion. On the other hand, in case some of dominated periods are on the *T* component ($\beta(\eta f) = \pi/2$) and the amplitudes on the *Z* component of the ground motion are very small, this situation is corresponding to the Love wave particle motion.

The second set of weighting factors depends upon the angle Ψ as a measure of the eccentricity of the Rayleigh orbit. On the *Z* and *R* components, the angle desired ($\theta = 0.21\pi$) is the one corresponding to a theoretical horizontal/vertical displacement ratio (~0.8) for fundamental long-period Rayleigh waves assuming the Gutenberg earth model [19]. This value is fairly close to what is actually found at installations on competent, massive rock. However, this weighting function will attenuate higher mode Rayleigh waves at the shorter periods (less than 10 sec), as well as short-period fundamental Rayleigh on incompetent surface layers. The amplitudes of the *Z* and *R* components are including unit weighting factor according as a function of $\cos^K\left[\psi(\eta f)-\theta\right]$ in the case of $\psi(\eta f) = \theta$. The amplitudes at the *T* component as to function of $\sin^K\left[\psi(\eta f)\right]$ are applied unit weighting for the case of perfectly horizontal motion ($\psi(\eta f) = \pi/2$). The amplitude values of the *R* and *Z* components are decreased by the function of $\sin^N\left[\alpha(\eta f)\right]$ in interval varied from 0 to 1 for fundamental mode Rayleigh waves.

The third weighting factor as a function of α attenuates the *Z* and *R* components by an amount which decreases from 1 to 0 as the phase departs from the theoretical 90˚ retrograde relationship for Rayleigh motion on a laterally homogeneous half space. No corresponding weight is possible for the *T* component. The process clearly will not work at all if Love and Rayleigh waves of similar frequency content (and comparable amplitudes) arrive in the same time segment. In such a case, the time and space patterns of both wave groups will be mutually confused, resulting in little or no output.

5) All three seismograms are reconstructed in the time domain using the weighted Fourier amplitude coefficients, $A'_Z(\eta f)$, $A'_R(\eta f)$ and $A'_T(\eta f)$ and the phase angles determined initially $\theta'_Z(\eta f)$, $\theta'_R(\eta f)$ and $\theta'_T(\eta f)$.

6) The filtered signal is obtained by using the arithmetic mean of overlapped amplitude values.

3. Application of Method

In this study, the surface wave discrimination filter based on polarization properties was applied to the broad-band digital three component seismograms recorded at eight stations (**Table 1**, **Figure 2**) having about 10˚ epicenter distances of Bogazici University Kandilli Observatory and Earthquake Research Institute (KOERI) for Erzurum earthquake occurred in Turkey. Focal parameters of Erzurum earthquake are given in **Table 2**. The time sampling is 1 sec. The magnifications of the three component seismograms are firstly equalized, then the horizontal axes are rotated as shown from **Figure 3(a)** to **Figure 10(a)**. The rotated seismograms are divided into simultaneous time segments of length T, then for each of the three directional components the amplitude and phase terms are computed by discrete Fourier series.

The apparent horizontal azimuth, $\beta(\eta f)$ of each harmonic is determined by Equation (3). A measure of the eccentricity of the particle motion ellipse, $\psi(\eta f)$ is also calculated by Equation (4), and the phase difference, $\alpha(\eta f)$ between the vertical and radial components is determined by Equation (5). The Fourier amplitude coefficients of each directional component, $A_R(\eta f)$, $A_T(\eta f)$ and $A_Z(\eta f)$ are then weighted according to the Equation (6). In these equations, *M*, *K*, *N* constants and the angle θ corresponding to horizontal/vertical displacement ratio have been valued as 8, 8, 4 and 0.8, respectively (as suggested by [1]). After, it is back-transformed to the time domain with original phase value and scaled amplitude values, $A'_Z(\eta f)$, $A'_R(\eta f)$ and $A'_T(\eta f)$. The same process is repeated for the other windowing by selected moving interval and this process is continued by scanning all of the signals. Finally, filtered signals are obtained as the arithmetic average of the overlapping amplitudes (**Figures 3(b)-10(b)**). It has been examined on records having to difference epicentre distance for several window length and moving interval (**Table 3**). The original and filtered three component seismograms of recorded at ISP (**Figure 3**), YLVX (**Figure 4**), ANTB (**Figure 5**), ISKB (**Figure 6**), BALB (**Figure 7**), MRMX (**Figure 8**), MLSB (**Figure 9**) and EDRB (**Figure 10**) stations are compared. The start of time axis is 19:33:00 at all records in figures.

Table 1. Information of stations used in the application.

Station Code	Coordinates (˚N)	(˚E)	Epicenter Δ(˚)	Azimuth Az(˚)
YLVX	40.34	29.22	8.16	90
MLSB	37.18	27.47	10.07	71
MRMX	40.36	27.35	9.59	89
ISP	37.49	30.31	7.82	70
ISK	41.04	29.04	8.33	95
EDRB	41.51	26.45	10.32	95
BALB	39.38	27.53	9.52	83
ANTB	36.54	30.39	8.15	63

Table 2. The focal parameters of Erzurum earthquakes used in the application.

Date (d m y)	**Origin Time** (h min sec)	Coordinates (˚N)	(˚E)	Focal Depth (km)	Magnitude Ms
25.03.2004	19:30:46.3	39.92	40.82	10	6.0

Table 3. Parameters used in the analysis.

Station Code	Epicenter Δ(km)	Data Length (sec)	Window Length (sec)	Window Length/ Moving Interval	Smoothing Operator
ISP	927	720	75	3.95	9
YLVX	928	950	75	3.95	9
ANTB	950	720	75	3.95	9
ISK	1011	720	90	4.10	7
BALB	1113	720	90	4.50	9
MRMX	1134	720	90	4.50	9
MLSB	1176	720	90	4.50	9
EDRB	1211	720	120	4.80	9

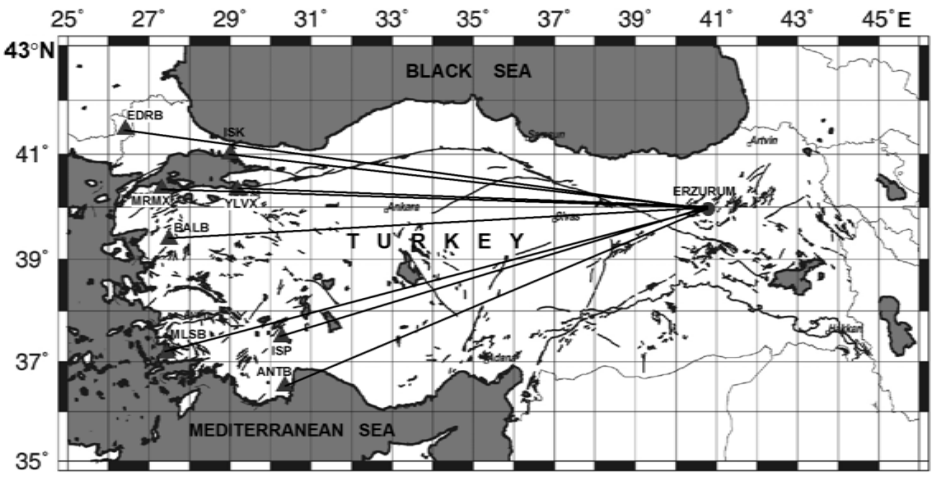

Figure 2. Location of the event (●) and stations (▲) are shown at tectonic map of Anatolia [20].

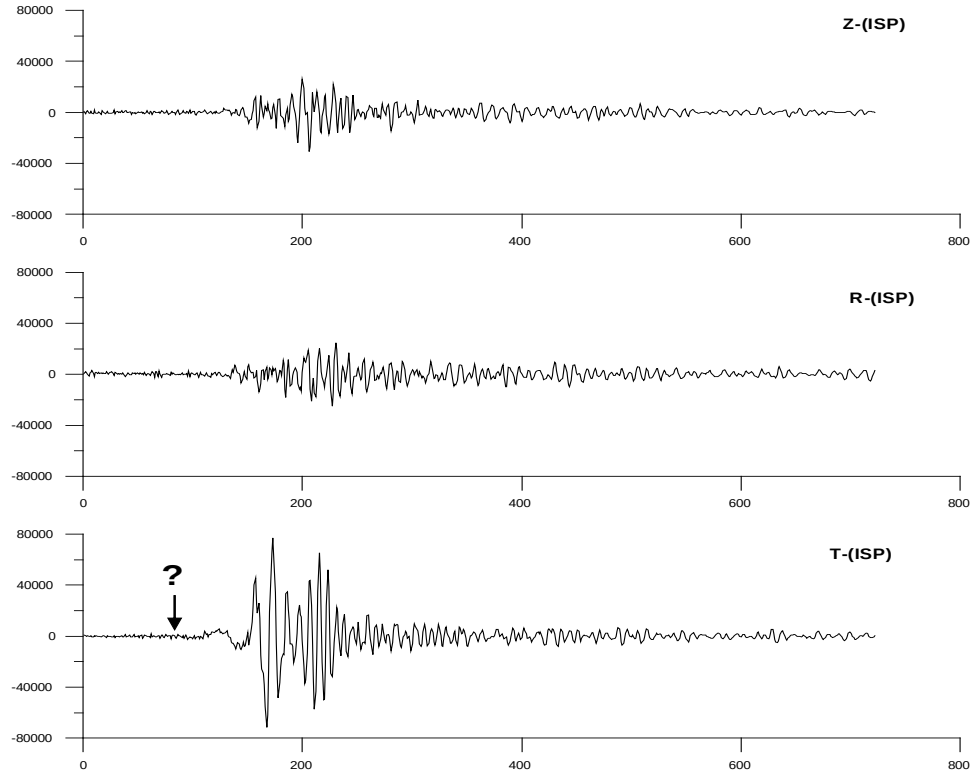

(a)

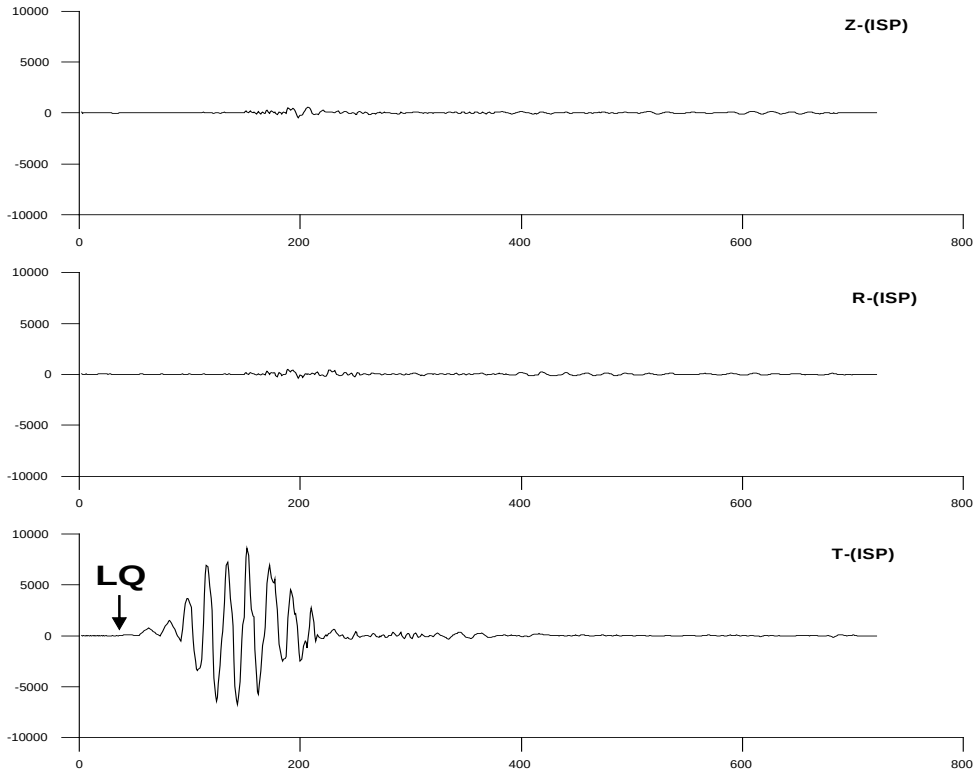

(b)

Figure 3. *Z*, *R* and *T* components recorded at ISP (Isparta) station. (a) Original records; (b) Filtered cases.

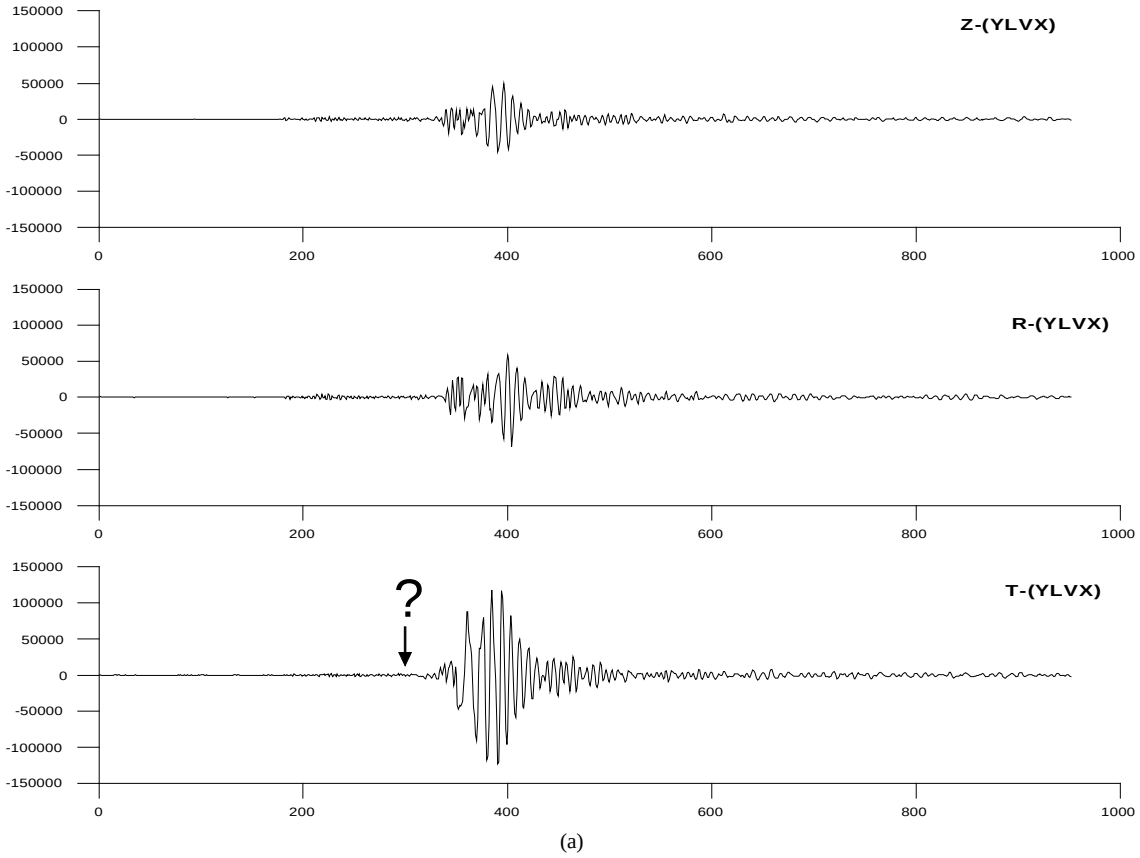

(a)

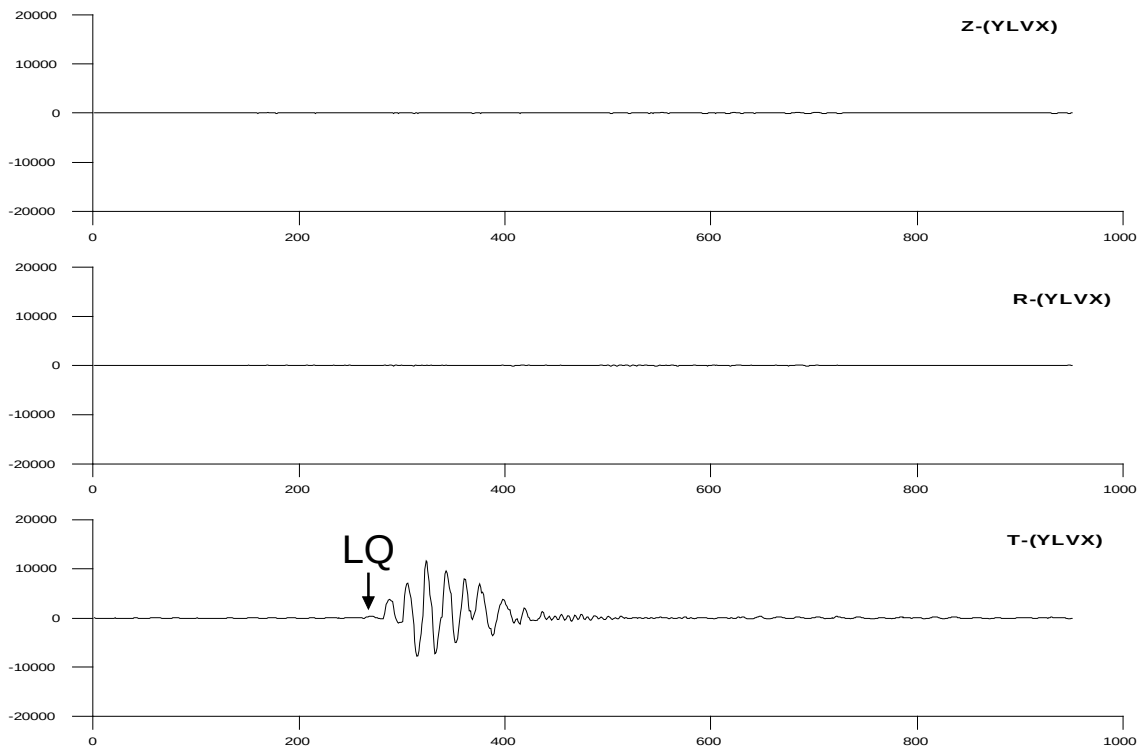

(b)

Figure 4. *Z*, *R* and *T* components recorded at YLVX (Yalova) station. (a) Original records, (b) Filtered cases.

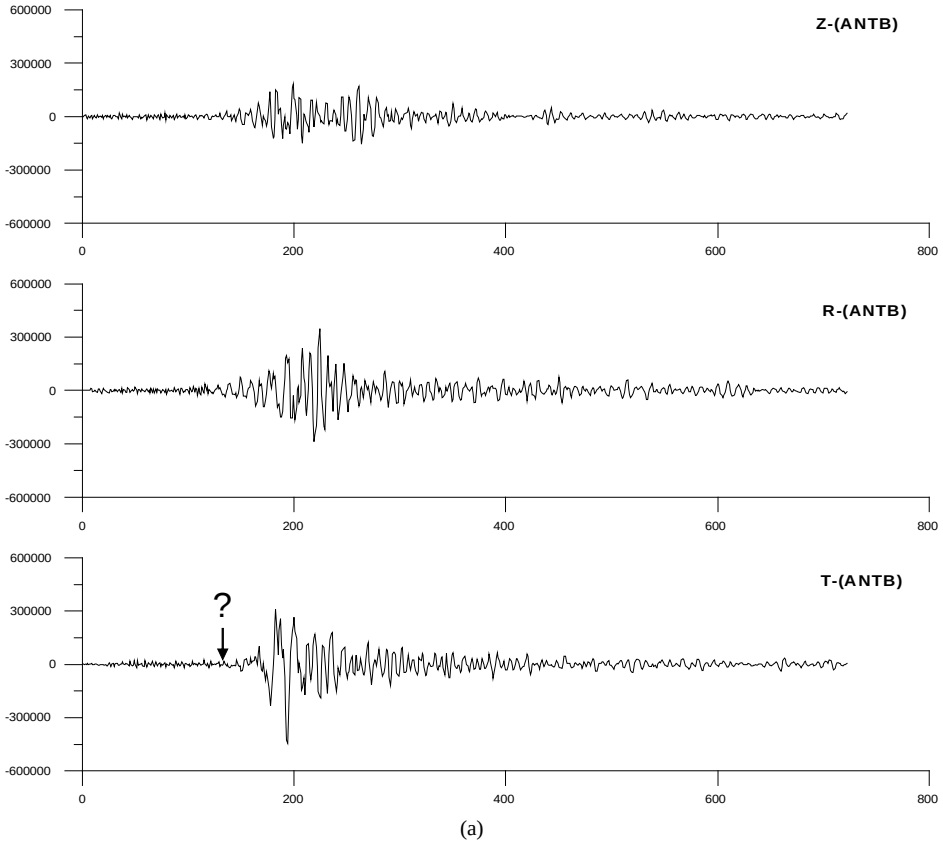

(a)

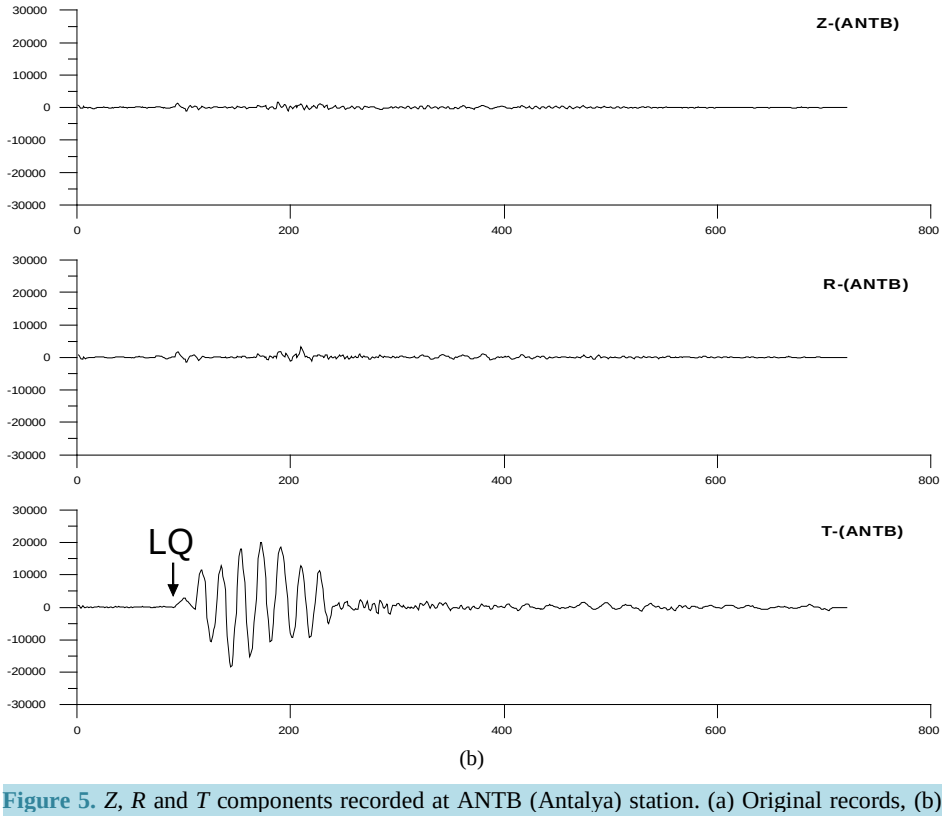

(b)

Figure 5. *Z*, *R* and *T* components recorded at ANTB (Antalya) station. (a) Original records, (b) Filtered cases.

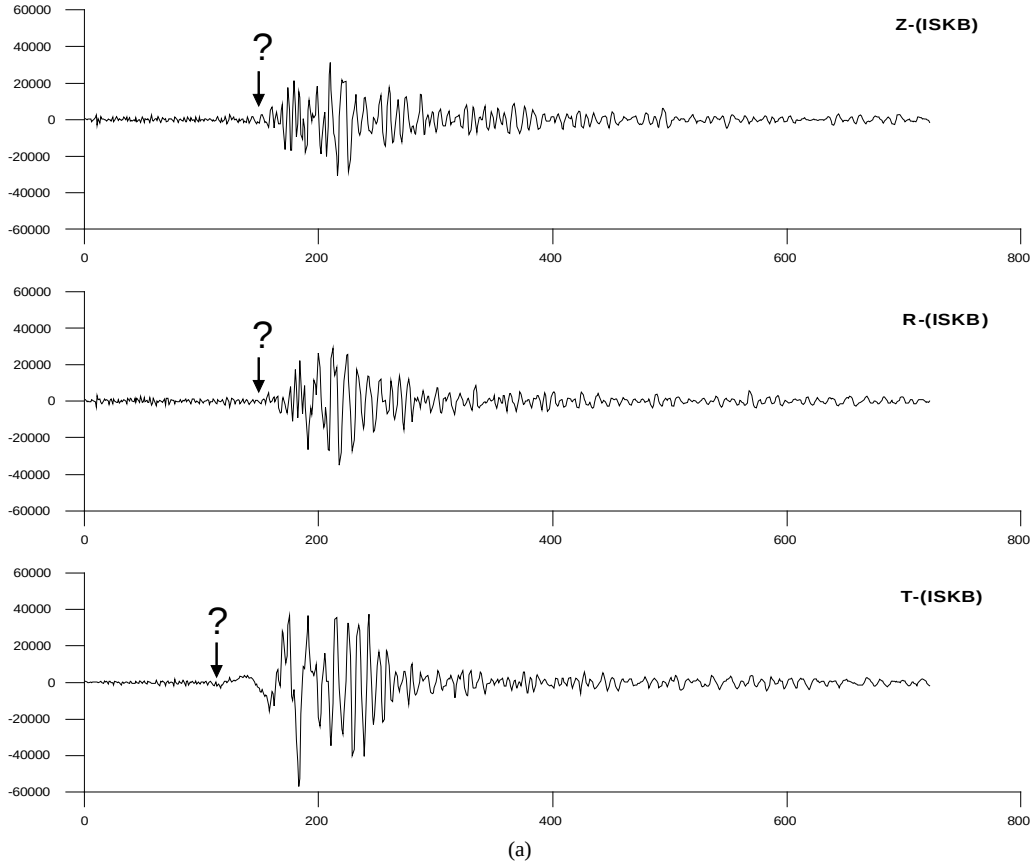

(a)

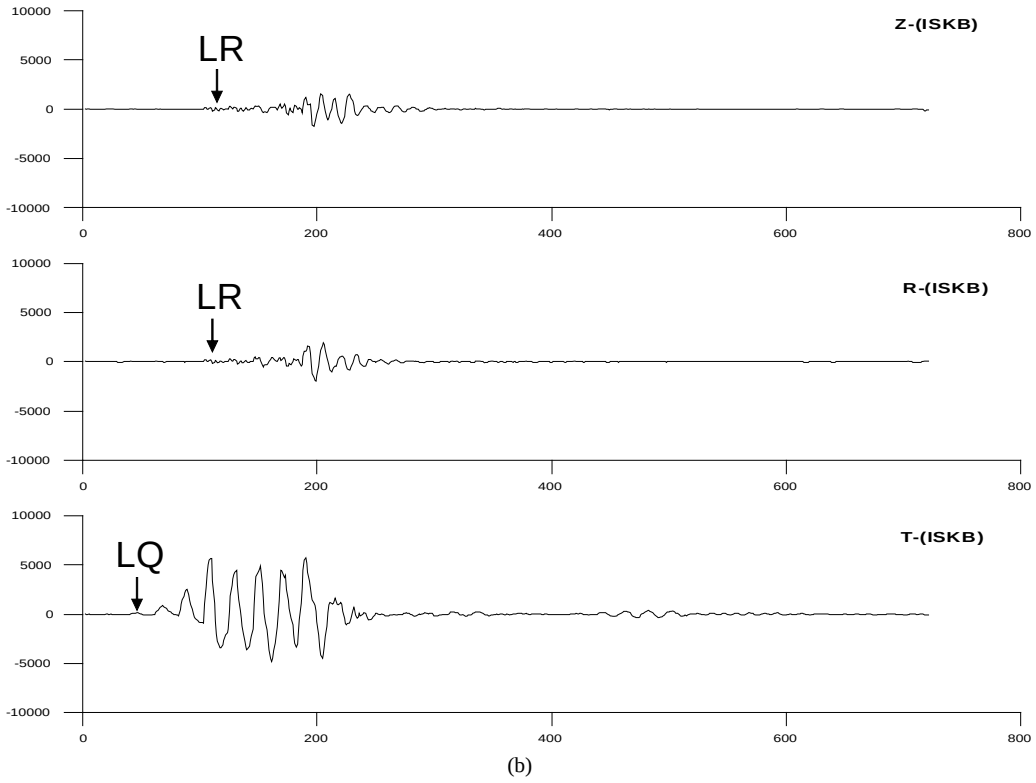

(b)

Figure 6. *Z*, *R* and *T* components recorded at ISKB (Istanbul) station. (a) Original records, (b) Filtered cases.

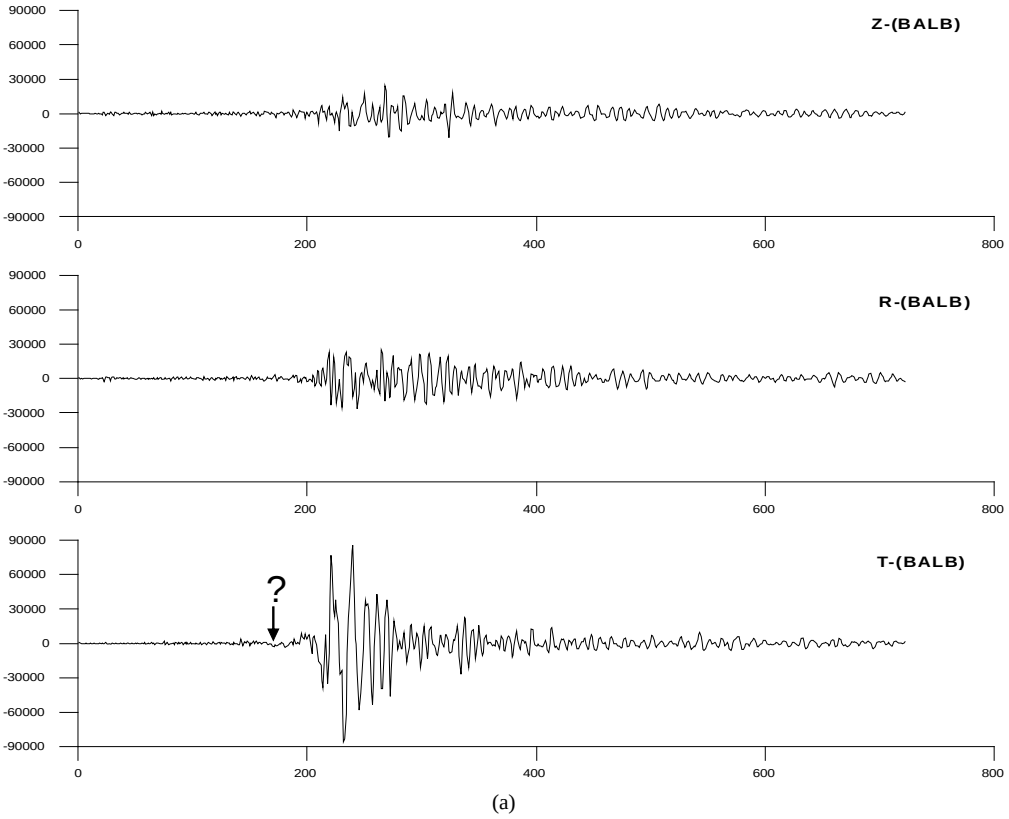

(a)

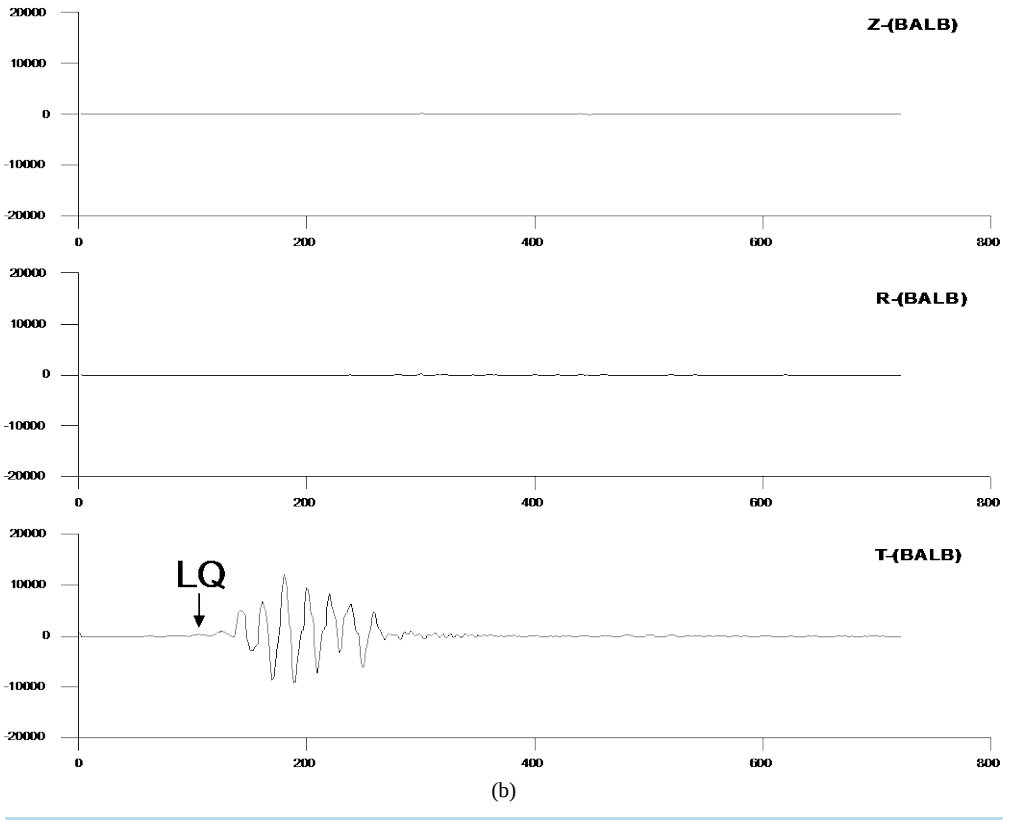

(b)

Figure 7. *Z*, *R* and *T* components recorded at BALB (Balıkesir) station. (a) Original records, (b) Filtered cases.

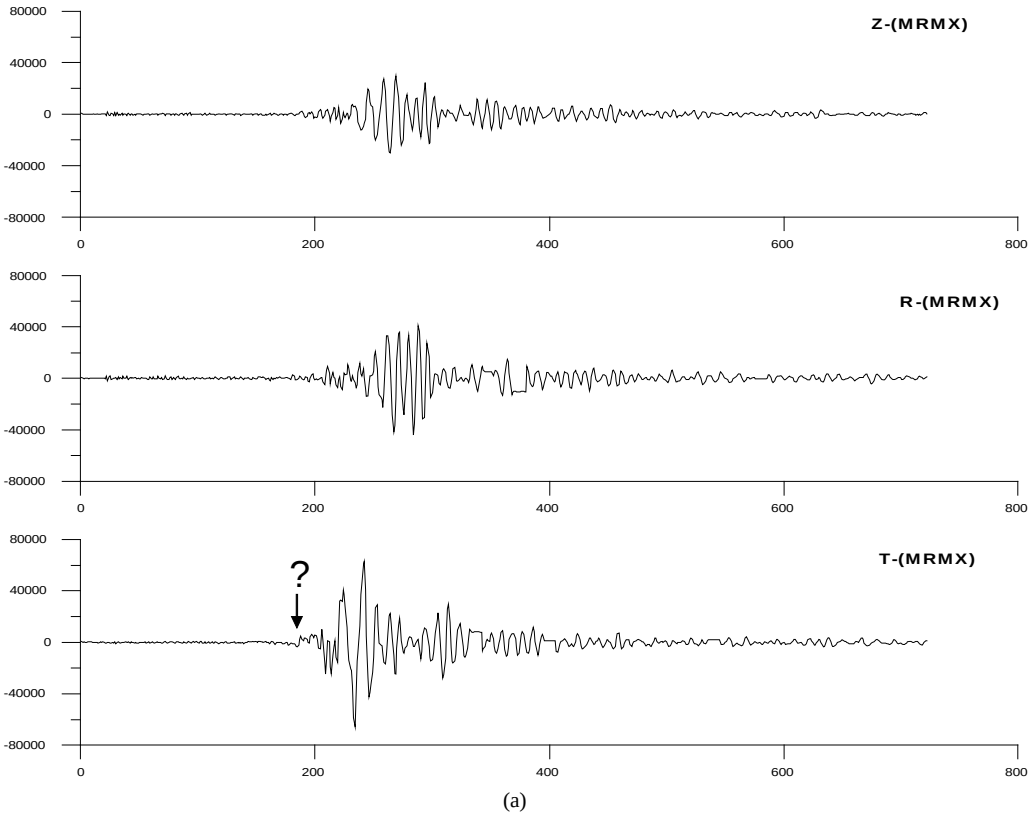

(a)

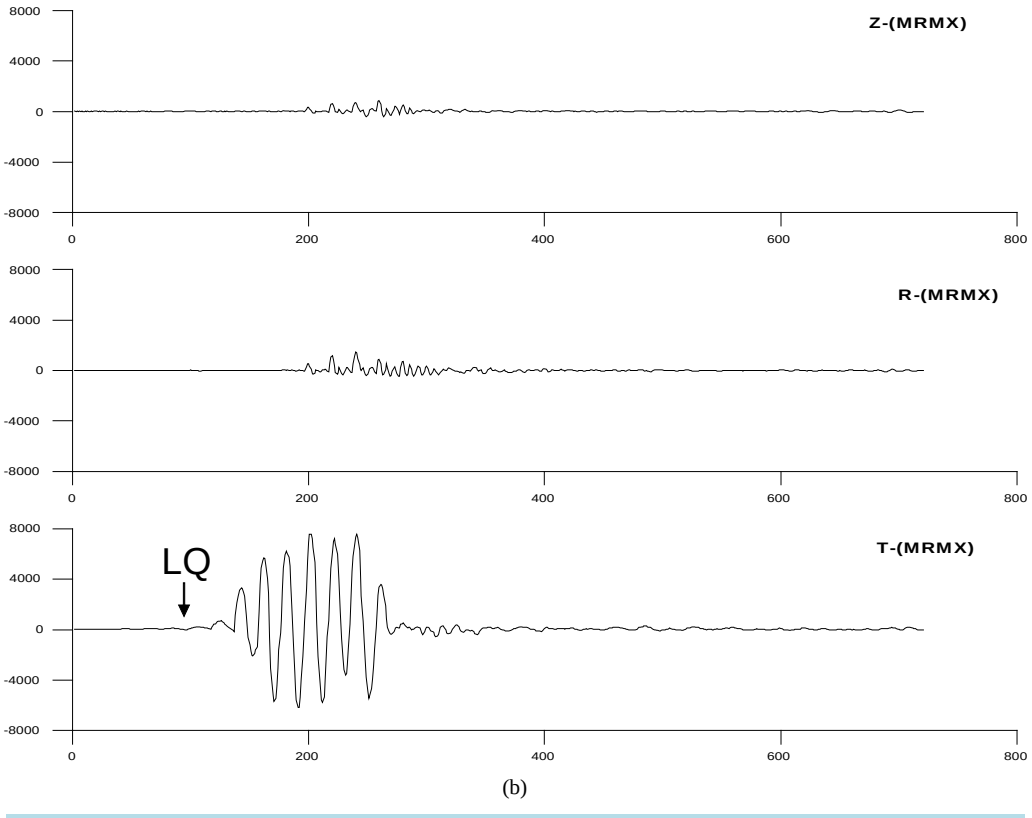

(b)

Figure 8. *Z*, *R* and *T* components recorded at MRMX (Marmara) station. (a) Original records, (b) Filtered cases.

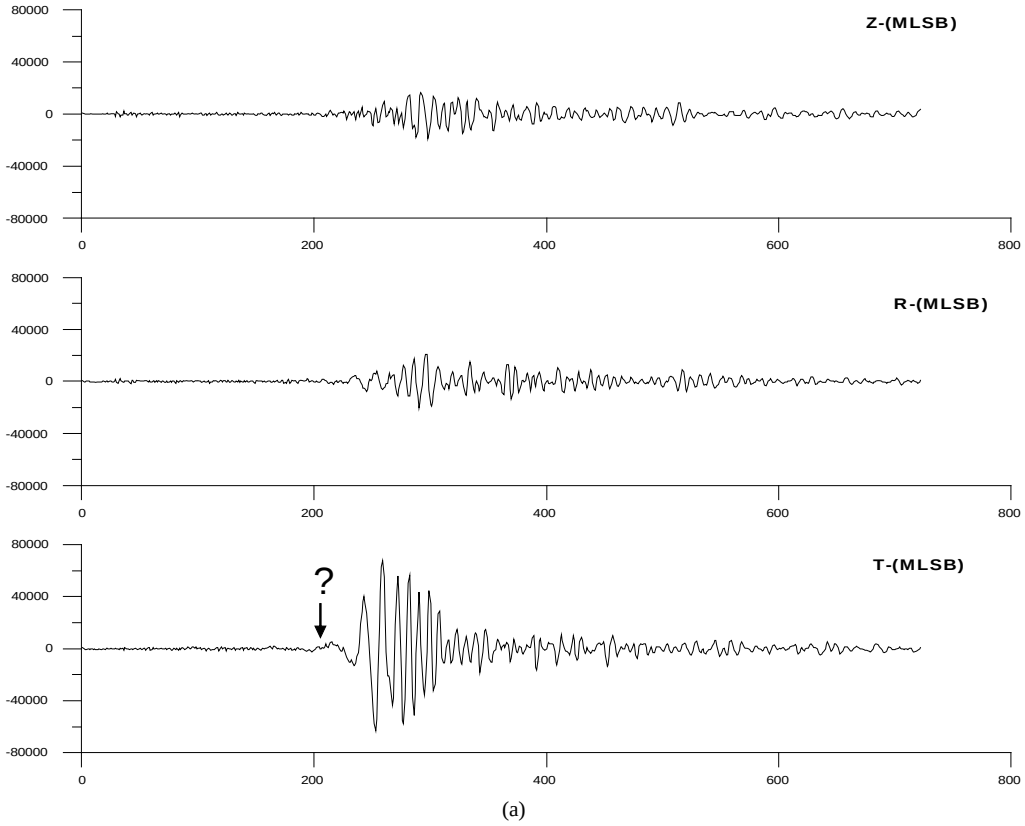

(a)

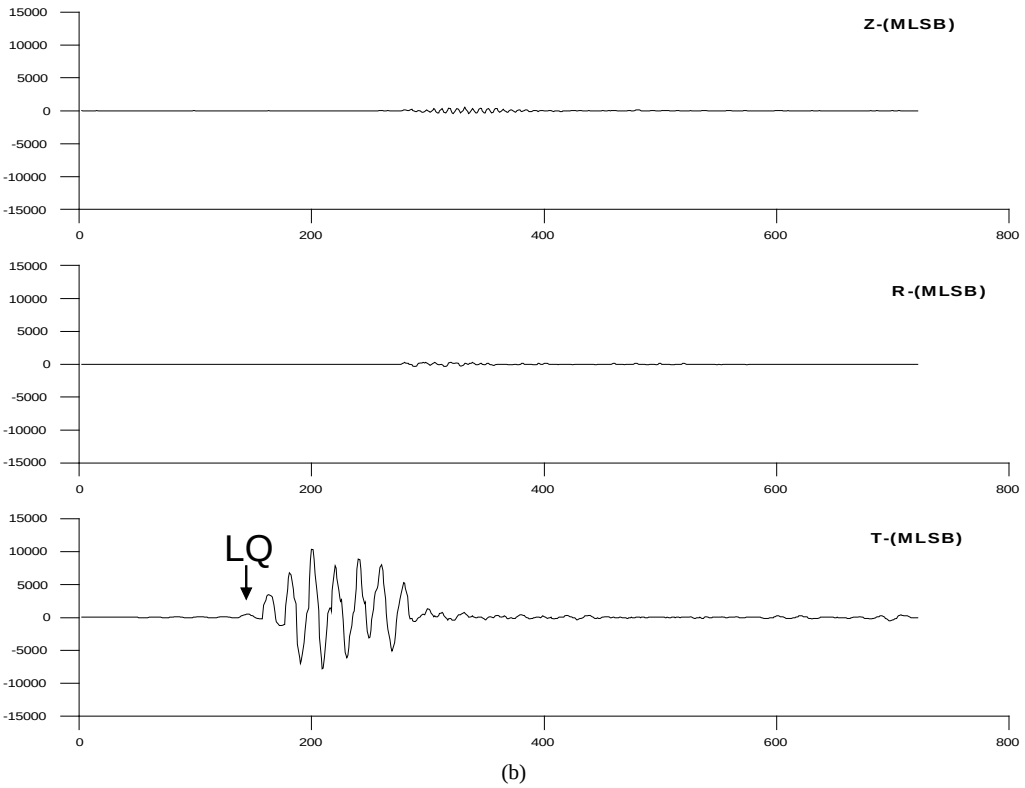

(b)

Figure 9. *Z*, *R* and *T* components recorded at MLSB (Bodrum) station. (a) Original records, (b) Filtered cases.

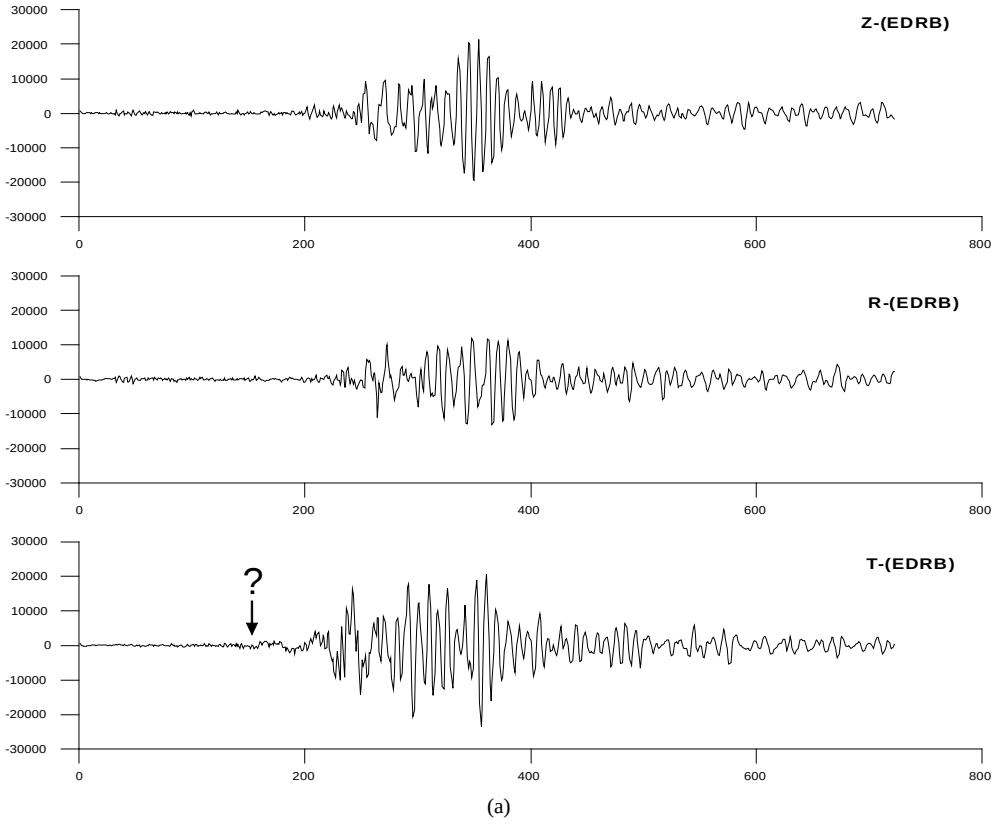

(a)

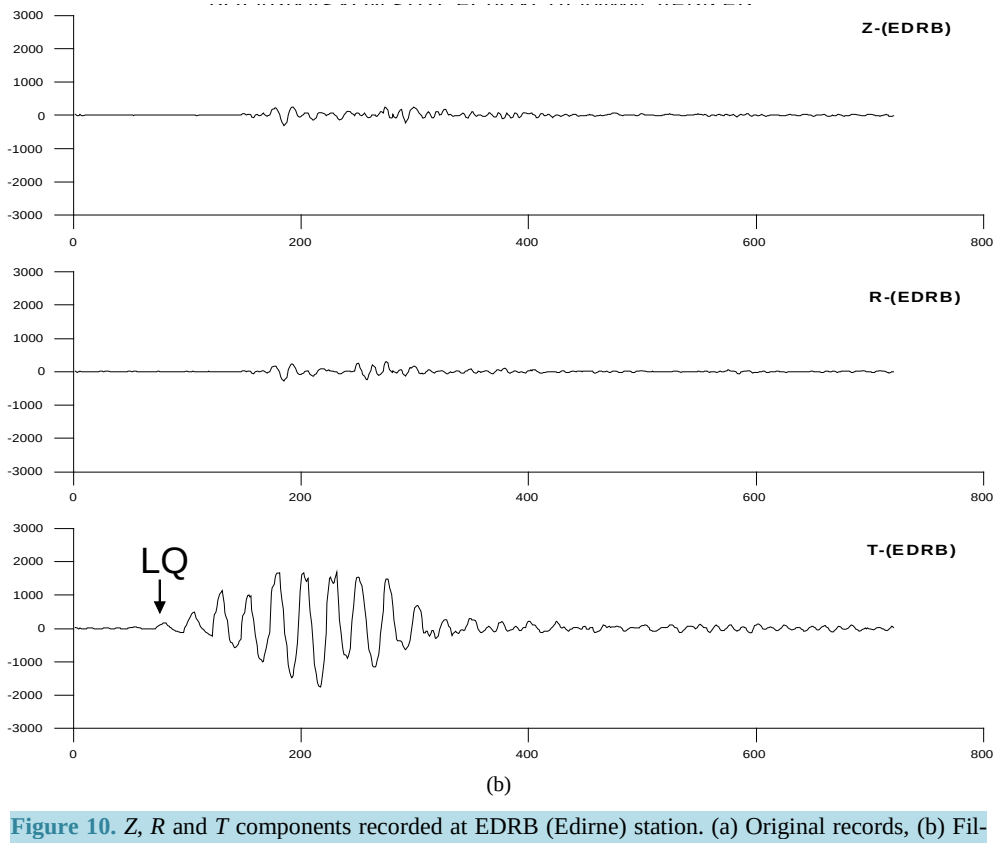

(b)

Figure 10. *Z*, *R* and *T* components recorded at EDRB (Edirne) station. (a) Original records, (b) Filtered cases.

4. Discussion and Conclusions

In this study, discrimination filter based on polarization properties has been applied to discriminate a desired surface wave phase on seismograms recorded at stations having about 10˚ of epicentre distances. For this purpose, three-component broadband digital seismograms recorded at eight stations of Bogazici University Kandilli Observatory and Earthquake Research Institute (KOERI) of Erzurum earthquakes were used and filtered seismograms were compared by original traces.

It has been found that the window length for the minimal epicentre distance (927 km) is 75 sec (for ISP) and, the window length for the maximal epicentre distance (1211 km) is 120 sec (for EDRB). As can be seen from analysed records, window length must be increased as related to the ascending epicentre distance (**Table 3**). Trials related to the surface wave discrimination filter technique have been denoted that window length and moving interval are significantly effect to the results. In this study, it has been determined that the ratio between the window length and moving interval is in the interval of 3.95 - 4.80 from the analysis of the records. References [6] and [11] have found the ratios of 4.4 and 3.0, respectively. Namely, the conclusions of present study agree with the results of the preview studies for different epicentre distances.

Love waves at records applied polarization filter have been obtained perfectly because the amplitudes on the tangential component (*T*) are larger than the amplitudes on the vertical (*Z*) and radial (*R*) components in all records (**Figures 3-10**). Dominate arrivals in some periods are on the *T* component and the amplitudes on the Z component of the ground motion are very small. Namely, total effect of weighting factors has been strengthened to Love waves at some periods arrive at the station. This result implies that the effects of the first weighting factors (functions of β) in Equation (6) are to attenuate transverse-tending energy on the *Z* and *R* components and radial-tending energy on the *T*-component. The directions of travel of obvious but unidentified Rayleigh groups at records have been determined by simply aiming the process for an azimuth angle about 90˚ and considering of the horizontal angles, β. Therefore, filter performance is low on *Z* and *R* components and in extracting the Rayleigh wave.

References

[1] Simons, R.S. (1968) A Surface Wave Particle Motion Discrimination Process. *Bulletin of Seismological Society of America*, **58**, 629-637.

[2] Gal'perin, E.I. and Frolova, A.V. (1960) Azimuth-Phase Correlation for Elliptically Polarized Waves, Izvestiya Soviet Academy of Sciences. *Geophysics Series*, **2**, 195-208. (in Russian)

[3] Shimsoni, M. and Smith, S.W. (1964) Seismic Signal Enhancement with Three Component Detectors. *Geophysics*, **24**, 664-671. http://dx.doi.org/10.1190/1.1439402

[4] Flinn, E.A. (1965) Signal Analysis Using Rectilinearity and Direction of Particle Motion. *Proceedings of IEEE*, **12**, 1874-1876. http://dx.doi.org/10.1109/PROC.1965.4462

[5] Mercado, B.J. (1968) Linear Filtering of Multicomponent Seismic Data. *Geophysics*, **33**, 926-935. http://dx.doi.org/10.1190/1.1439986

[6] Basa, S.H., Ozer, M.F., Osmansahin, I. and Kenar, O. (1994) Polarization Analysis of Three Component Data. *Geophysics*, **8**, 77-89.

[7] Alkaz, V.G., Onofrash, N.I. and Perelberg, A.I. (1977) Polarization Analysis of Seismic Waves. Shtiintca Press, Kishinev. (in Russian)

[8] Esmersoy, C. (1984) Polarization Analysis, Rotation and Velocity Estimation in Three Component VSP. In: Toksoz, M.N. and Stewart, R.R., Eds., *Vertical Seismic Profiling—Part B*: *Advanced Concepts*, Geophysical Press, Houston, 236-255.

[9] Jurkevics, A. (1988) Polarization Analysis of Three Component Array Data. *Bulletin of Seismological Society of America*, **78**, 1725-1743.

[10] Perelberg, A.I. and Hornbostel, S.C. (1994) Applications of Seismic Polarization Analysis. *Geophysics*, **59**, 119-130. http://dx.doi.org/10.1190/1.1443522

[11] Osmansahin, İ., Özer, M.F. and Sayil, N. (1994) Surface Wave Discrimination Filter Based on Polarization Properties. *Geophysics*, **8**, 99-104.

[12] Zheng, Y. (1995) Seismic Polarization Filtering: Noise Reduction and Off-Line Imaging. MSC, University of Galgary, Galgary.

[13] Patane, D. and Ferrari, F. (1999) ASDP: A PC-Based Program Using a Multi-algorithm Approach for Automatic De-

tection and Location of Local Earthquakes. *Physics of the Earth Planetary Interiors*, **133**, 57-74. http://dx.doi.org/10.1016/S0031-9201(99)00030-8

[14] Du, Z., Foulger, G.R. and Weijian, M. (2000) Noise Reduction for Broad-Band, Three Component Seismograms Using Data-Adaptive Polarization Filters. *Geophysical Journal International*, **141**, 820-828. http://dx.doi.org/10.1046/j.1365-246x.2000.00156.x

[15] Franco, R. and Musacchio, G. (2001) Polarization Filter with Singular Value Decompozition. *Geophysics*, **66**, 932-938. http://dx.doi.org/10.1190/1.1444983

[16] Kutlu, Y.A. (2006) Surface Wave Discrimination Filter Based on Polarization Properties and Its Applications. Ph.D. Thesis, Karadeniz Technical University, Trabzon.

[17] Kutlu, Y.A. and Sayil, N. (2013) The Modified Surface Wave Particle Motion Discrimination Process. *International Journal of the Physical Sciences*, **8**, 395-405.

[18] Haubrich, R.A. and McKenzie, G.S. (1965) Earth Noise 5 to 500 Millicycles per Second. Part 2. *Journal of Geophysical Research*, **70**, 1429-1440. http://dx.doi.org/10.1029/JZ070i006p01429

[19] Dorman, J. and Prentiss, D. (1960) Particle Amplitude Profiles for Rayleigh Waves on a Heterogeneous Earth. *Journal of Geophysical Research*, **65**, 3805-3816. http://dx.doi.org/10.1029/JZ065i011p03805

[20] Saroglu, F., Emre, O. and Kuscu, I. (1992) Active Fault Map of Turkey. General Directorate of Mineral Research and Exploration, Ankara.